

In Situ Photoactivated Plasmonic Ag₃PO₄@silver as a Stable Catalyst With Enhanced Photocatalytic Activity Under Visible Light

Dongfang Zhang^{a*}, Jiaxun Wang^a

^aCollege of Science, Huazhong Agricultural University, Wuhan 430070, P.R. China

Received: October 26, 2016; Revised: February 11, 2017; Accepted: March 09, 2017

Silver orthophosphate (Ag₃PO₄) had been reported as an excellent candidate to split water or decompose pollutants with high efficiency in visible light region, yet is not stable due to the reduction of silver ion. In this work, an easy-fabricated method (*in situ* photoinduced reduction) was provided to enhance the stability of Ag₃PO₄ for its possible application as a visible-light sensitive photocatalyst. The as-prepared samples were characterized by X-ray diffraction (XRD), UV-vis diffuse reflectance spectra, photoluminescence spectra (PL) and Photoelectrochemical measurements. The Ag₃PO₄/Ag photocatalysts showed strong photocatalytic activity for decomposition of RhB dye or phenol-X-3B mixture under visible light irradiation ($\lambda > 420$ nm) and can be used repeatedly. The possible mechanism for the enhanced photocatalytic properties of the Ag₃PO₄/Ag hybrid was also discussed. It was found that $\bullet\text{OH}$ and holes take priority over $\bullet\text{O}_2^-$ radicals in serving as the main oxidant in the Ag₃PO₄/Ag photocatalytic system. Especially, the experimental results indicate that the surface plasmon resonance of Ag nanoparticles and a large negative charge of PO₄³⁻ ions as well as high separation efficiency of e^- - h^+ pairs, facilitated the enhancement of the photocatalytic activity of the Ag₃PO₄/Ag composite. The results indicated that Ag₃PO₄/Ag is an efficient and stable visible-light-driven photocatalyst.

Keywords: Silver phosphate; Photocatalytic; Cycle test; Phenol degradation

1. Introduction

In recent years, heterogeneous photocatalysis has attracted considerable attention as a promising “green” technology for solving environmental problems as well as providing renewable energy sources. The environmental problem caused by organic pollutants has increased with the rapid development of industry and become a severe threat to human beings¹. In this regard, semiconductor photocatalysis is one of the advanced physicochemical processes applicable in the photodegradation of environmental organic pollutants and toxic materials. The basic concept of semiconductor photocatalysis involves generation of electrons in the conduction band and holes in the valence band in a semiconductor on light irradiation at an energy equal to or higher than the bandgap of the semiconductor. Subsequently, photoexcited charge carriers are utilized to initiate redox reactions with suitable substrates on and/or near the semiconductor surface. However, the unavoidable fast recombination of photogenerated charge carriers in the semiconductor decreases the photocatalytic efficiency. Competition between the transfer and recombination processes of photogenerated charge carriers is therefore an important factor determining the photocatalytic performance of semiconductors.

Among various oxide semiconductor photocatalysts, TiO₂ was the most studied one due to its biological and chemical dormancy, non-toxicity, strong oxidizing activity

and long-term chemical stability²⁻⁶. However, TiO₂ mainly absorbs ultraviolet light (UV light) with wavelengths <380 nm, which covers only 5% of the solar spectrum, due to its wide band-gap of 3.2 electron volt (eV). Therefore, it is of great interest to develop a new visible-light photocatalysts to extend the absorption wavelength range into the visible-light region. So far, a successful example of suppressing electron-hole recombination is to deposit metal nanoparticles (NPs) on semiconductors. The noble metal (e.g., Au, Ag, Pt) in semiconductor/metal heterostructures, which acts as a reservoir for photogenerated electrons, promotes an interfacial charge-transfer process because of its high Schottky barrier at the metal/semiconductor interface^{7,8}. The transfer of photoinduced electrons from noble metal to semiconductor is also of special interest, because this process offers effective utilization of sunlight owing to the strong surface plasmon resonance (SPR) of metal NPs. This resonance is a consequence of enhancement of the local electromagnetic field due to the resonant response of the metal electrons at specific wavelengths, which strongly depends on the morphology and size of the NPs, composition, as well as the dielectric properties of the surrounding medium⁹. On absorption of a photon at the plasmon resonance frequency, coherent oscillations in the free electrons are induced, so an alternating electric field near the metal NPs is established. SPR can dramatically amplify visiblelight absorption, and therefore metal NPs could be utilized as a kind of visible-light harvesting and

* e-mail: zdfbb66@aliyun.com

converting centers to develop new plasmon-enhanced photocatalysts. Recently, it was reported that the new use of Ag₃PO₄ semiconductor in photocatalytic applications, where it exhibits extremely high photooxidative capabilities for the O₂ evolution from water and the decomposition of organic dyes under visible-light irradiation. More specifically, this novel photocatalyst can achieve a quantum efficiency of up to 90% at wavelengths greater than 420 nm¹⁰. Moreover, it was demonstrated theoretically that the Ag vacancies with a high concentration in Ag₃PO₄ have a significant effect on the separation of electron–hole pairs and optical absorbance in the visible-light region¹¹. However, Ag₃PO₄ is photosensitive intrinsically. Silver orthophosphate grain absorbs a photon to generate an electron and a hole, and then the electron combines with an interstitial silver ion to give a silver atom. Therefore, it is a highly crucial task to improve the photocatalytic stability of Ag₃PO₄ while maintaining its high photocatalytic activity.

In this work, trisodium citrate was used as chelating agent and NaH₂PO₄ was used as precipitating agent in the wet chemical reaction route to synthesize visible-light-active Ag₃PO₄/Ag plasmonic photocatalyst with the purpose of improving the stability of Ag₃PO₄. It is well-known that the citric acid can be served as a chelating agent to form immediate Ag⁺–Cit³⁻ complex for the next preparation of Ag₃PO₄, whereas Na₃Cit possesses three carboxyl groups (–COO) and one hydroxyl group (–OH) that can serve as binding sites. These features not only provide Na₃Cit with a strong chelating ability and a superior capping capability, but also help to improve self-aggregation of complex hierarchical structures via formation of Ag₃Cit precursors, homogeneous nucleation of Ag₃PO₄ via dissolution of the precursor, and growth into porous structures through an insideout Ostwald ripening process^{12–14}. Since the SPR effect of silver nanoparticles and a large negative charge of PO₄³⁻ ions, the reducibility of Ag⁺ ions in the Ag₃PO₄ lattice decreased significantly when the surface of Ag₃PO₄ is covered by Ag⁰ nanoparticles. Thus, the highly efficient and stable photocatalyst is obtained. The photocatalytic properties of as-prepared Ag₃PO₄/Ag plasmonic photocatalyst were described for their applications in degrading typical organics. Rhodamine-B (RhB), phenol and X-3B, were used as the target pollutants in aqueous media to assess the photocatalytic activity of the Ag/Ag₃PO₄ plasmonic photocatalyst. Additionally, the mechanism of photocatalytic degradation of phenol over the Ag/Ag₃PO₄ plasmonic photocatalyst was also proposed. Besides, it is well known that Ag₃PO₄ is a visible-light responsive photocatalyst. In order to get significant information about the visible-light-driven activity of as-prepared Ag₃PO₄/Ag nanohybrid, it is also important to compare it with that to other visible-light-induced photocatalyst such like nitrogen doped TiO₂.

2. Materials and Methods

2.1. Materials preparation

All chemical reagents utilized in the present work were analytical grade reagents purchased from Guoyao Chemical Corporation obtained and used without further purification. Deionized water was used throughout. In a typical synthesis, 30 mL of AgNO₃ (0.12 M) was added into 30 mL aqueous solution containing 4.5 mmol of trisodium citrate (labeled as Na₃Cit herein) to form the immediate Ag⁺–Cit³⁻ complex at room temperature. The resulting white turbid mixture was agitated for another 60 min, 60 mL of aqueous solution containing 1.5 mmol NaH₂PO₄ was introduced into the above solution. Under magnetic stirring for 3.0 h, the color of the reaction solution was observed to change gradually from white turbid to bright yellow. At last, the yellow precipitates were collected by centrifugation, thoroughly rinsed repeatedly several times with absolute ethanol and distilled water, and then dried at room temperature for 24 h to obtain the final Ag₃PO₄ nanoparticles. Ag₃PO₄/Ag photocatalyst was further prepared by light-induced method. In brief, the obtained Ag₃PO₄ was dispersed into a solution of methylene blue (MB) dye and irradiated with a 300 W Xe lamp for 2 h. The distance between the light source and the reactor during the photodeposition process is adjusted to about 12 cm. The color of sample changed from yellow to dark grey, which indicated the transformation of part of the Ag₃PO₄ into Ag and the generation of Ag₃PO₄/Ag nanocomposites. Then the photocatalysts were collected by centrifugation, thoroughly rinsed repeatedly several times with absolute ethanol and distilled water, and dried at 50°C for 24 h in the dark to obtain the final Ag₃PO₄/Ag nanoparticles. For comparison, N-doped TiO₂ (N-TiO₂) reference photocatalyst was prepared by nitridation of commercially available TiO₂ powder (surface area 50 m²/g) at 773 K for 12 h under NH₃ flow (flow rate 300 mL/min).

2.2. Characterization

To determine the characterizations of the samples, various devices and equipments were used. The crystallinity and phase of the samples were analyzed by XRD diffractometer using Cu K_α (λ = 1.5406 Å) radiation. The UV-vis absorption spectra was obtained with a UV-vis spectrophotometer (Shimadzu 2450 PC) was mounted with an integrating sphere accessory (ISR1200) using BaSO₄ as reference standard was used to investigate the light absorption and optical band gap of the synthesized film samples (the wavelength range was varied from 200–800 nm). Photoluminescence spectra (PL) were measured at room temperature on a SHIMADZU RF-5301 PC spectrometer using (excitation light E_x = 280 nm, emission spectrometry range E_M = 320–800 nm).

Photoelectrochemical measurements were performed using a conventional three-electrode cell system and a CHI 760C (CHI Co., USA) electrochemical workstation. The $\text{Ag}_3\text{PO}_4/\text{Ag}/\text{ITO}$ electrode was employed as the working electrode, while $\text{Ag}_3\text{PO}_4/\text{Ag}/\text{ITO}$ electrode was prepared as follows: 0.20 mg of $\text{Ag}_3\text{PO}_4/\text{Ag}$ sample was added in ethanol (20 mL) and sonicated for 30 min, then indium tin oxide (ITO) glass substrates (3 cm \times 2 cm) with a sheet resistance of 15 Ω were dipped into the complex precursor for 10 min and then were pulled out with a velocity of 3 cm \cdot min $^{-1}$. Then the sample was dried at 50 $^\circ\text{C}$ for 12 h. Meanwhile, a platinum electrode and a saturated calomel electrode served as the counter and reference electrode, respectively. The working electrode was irradiated by visible light (420 nm $< \lambda$) through a UV-cutoff filter (Shanghai Seagull Colored Optical Glass Co., Ltd.) from a high-pressure xenon short arc lamp (a Phillips 300 W Xe lamp). The incident light intensity of the visible light was 30.2 mW cm $^{-2}$) which was measured with a radiometer. The electrochemical impedance spectroscopy (EIS) was carried out in the frequency range of 10^{-2} to 10^5 Hz with an ac voltage amplitude of 10 mV at a dc bias of 0.3 V vs the saturated calomel electrode (SCE) in a 0.01 M Na_2SO_4 electrolyte.

2.3. Photocatalytic degradation experiment.

After synthesis and characterization, the photocatalytic activity of as-prepared $\text{Ag}_3\text{PO}_4/\text{Ag}$ sample was tested under visible light irradiation for the degradation of target pollutants in water. The photocatalytic activities were evaluated by the decomposition of RhB dye under visible light ($\lambda > 420$ nm). The visible light was obtained by a 300 W xenon lamp (Institute of Electric Light Source, Beijing) with a 420 nm cutoff filter to ensure the desired irradiation light. The distance between the liquid surface and the light source was about 10 cm. The photocatalyst obtained by a typical experiment was dispersed into an aqueous solution of the organic pollutant (100 mL, 20 mgL $^{-1}$) in a beaker by sonication. The solution that contained the organic pollutant and the photocatalyst was stirred continuously for 50 min in the dark to ensure the establishment of an adsorption/desorption equilibrium among the photocatalyst, organic pollutant, and water before light irradiation. During the degradation, the mixture was stirred continuously by means of a magnetic stirrer. At certain time intervals, 5 mL aliquots were sampled and centrifuged to remove the particles. The filtrates were analyzed by recording variations of the maximum absorption band (553 nm for RhB) using a Hitachi U-3010 UV-vis spectrophotometer.

2.4. Detection of hydroxyl radicals.

The formation of hydroxyl radical ($\bullet\text{OH}$) on the surface of photoirradiated $\text{Ag}_3\text{PO}_4/\text{Ag}$ sample is detected by photoluminescence (PL) technique using terephthalic acid as

a probemolecule. Terephthalic acid readily reacts with $\bullet\text{OH}$ to produce highly fluorescent product, 2-hydroxyterephthalic acid. The typical experimental procedures are as follows. The sample was placed in a 50 mL aqueous solution of 3.0×10^{-4} mol L $^{-1}$ terephthalic acid and 4×10^{-4} mol L $^{-1}$ NaOH in a beaker at ambient temperature, and put in the same xenon lamp as the light source at the intervals of irradiation time (0, 10, 20, 30, 40 and 50 min). A 5 ml of the suspension was collected. PL spectra of the 2-hydroxy terephthalic acid produced by the reaction between terephthalic acid and photogenerated hydroxyl radicals were recorded on a Shimadzu RF-5301 PC spectrometer using Excitation wavelength of 315 nm ($E_x = 315$ nm), and scanning light wavelength of 350–600 nm ($E_M = 350 - 600$ nm).

3. Results and Discussion

The crystal structure and crystal phase characterization of the samples were first investigated by X-ray diffraction (XRD). Ag_3PO_4 is a body-centred cubic structure with a lattice parameter of 0.6 nm, consists of isolated and regular PO_4 tetrahedral (P O distance of ~ 0.15 nm) to form a body-centred cubic lattice and six Ag^+ ions are distributed among twelve sites of two-fold symmetry, while the O atoms possess 4-fold coordination surrounded by three Ag atoms and one P atoms. As can be seen from Figure 1, the X-ray diffraction (XRD) patterns of Ag_3PO_4 sample obtained before visible-light irradiation, show that the diffraction peaks of the sample before irradiation could be indexed to the body-centered cubic structure of Ag_3PO_4 . The distinct diffraction peaks at $2\theta = 20.9^\circ, 29.7^\circ, 33.4^\circ, 36.7^\circ, 47.9^\circ, 52.8^\circ, 55.1^\circ$ and 57.4° corresponding to the (110), (200), (210), (211), (222), (320) and (321) crystal planes were identified and can be assigned to the pure phase of well-crystallized cubic Ag_3PO_4 (space group P43n)¹⁵. The strong and sharp diffraction peaks indicate the high crystallinity of the product. All patterns matched very well with the JCPDS no. 06-0505 standard data of Ag_3PO_4 . As for $\text{Ag}_3\text{PO}_4/\text{Ag}$ sample which was prepared through light-induced method for pristine Ag_3PO_4 , the diffraction peaks located at $38.1^\circ, 44.3^\circ, 64.3^\circ$ and 77.5° can be attributed to the (111), (200), (220) and (311) planes of metallic Ag (JCPDS file no. 04-0783), respectively, which were marked with “■” in the graph. In addition, no other peaks of impurities or other phases such as Ag_2O are observed in XRD patterns of $\text{Ag}_3\text{PO}_4/\text{Ag}$ composites, indicating that the samples only contain the metallic Ag and Ag_3PO_4 . The XRD pattern of as-prepared N-TiO $_2$ sample that was prepared at calcination temperature of 500 $^\circ\text{C}$ was also shown in the same graph. Five high-intensity crystal peaks at $2\theta = 25.3^\circ, 38.0^\circ, 48.1^\circ, 53.8^\circ, 54.8^\circ$ and 62.8° can be perfectly indexed as (101), (004), (200), (105), and (211) crystal planes of anatase phase (JCPDS, NO. 21-1272), respectively. However, a small peak centered at $2\theta = 27.4^\circ$ corresponding to the (110) plane diffraction of rutile crystalline structure appear,

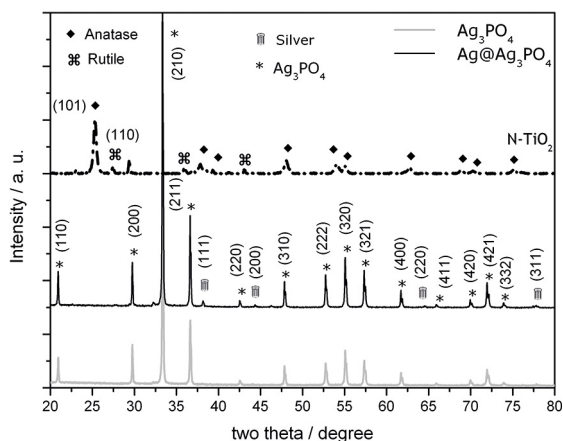


Figure 1. XRD patterns of the as-prepared Ag₃PO₄, Ag₃PO₄/Ag and N-TiO₂ samples.

which means that the rutile phase was already formed on the surface of anatase TiO₂ particles when the heat treatment temperature reached 500°C. Therefore, the as-prepared N-TiO₂ sample in the experimental condition should be mixed-phase nanocrystalline titania. Crystallite size of Ag₃PO₄ before and after Ag deposition should be mentioned and discussed. Therefore, average crystallite size of as-prepared catalysts were estimated according to Scherrer's formula: $d = m\lambda / (b \cos(2\theta))$, where d was the average grain size (nm), λ was the wavelength of the Cu-K α applied ($\lambda = 0.15406$ nm), θ was the Bragg's angle of diffraction, b was the full-width at half maximum intensity of the peak, m is the shape constant of crystal. Assign {210} main peak of XRD pattern that used in calculation of crystallite size by above scherrer equation, the average crystallite sizes of Ag₃PO₄ and Ag₃PO₄/Ag were estimated to be 26.0 nm and 32.0 nm, respectively. The results indicate that Ag₃PO₄/Ag sample is certainly slight agglomerate compared to fine Ag₃PO₄ particles where some of the agglomerate still is nanometer sized.

It is well known that the photocatalytic activity of a semiconductor is related with band gap energy. The optical absorption properties play a critical role in determining the photocatalytic performance of a catalyst, especially for the visible-light-driven photodegradation of organic contaminants. Figure 2 shows the UV-vis diffuse reflectance spectra of the as-prepared Ag₃PO₄, Ag₃PO₄/Ag and the reference N-TiO₂ powders. For the absorption spectrum of the reference N-TiO₂ sample, the first edge is related to the band structure of mixed-phase TiO₂ while the second one is probably due to the presence of a midgap band located above the valence band. This higher energy level arising from the localized N 2p states in the band structure. Therefore, the N-doped TiO₂ sample exhibits a red shift in the band gap transition compared with pure titania and remarkably expands the wavelength response range to the visible light region. The corresponding N 2p interface states, which are located above the valence band edge, significantly interact

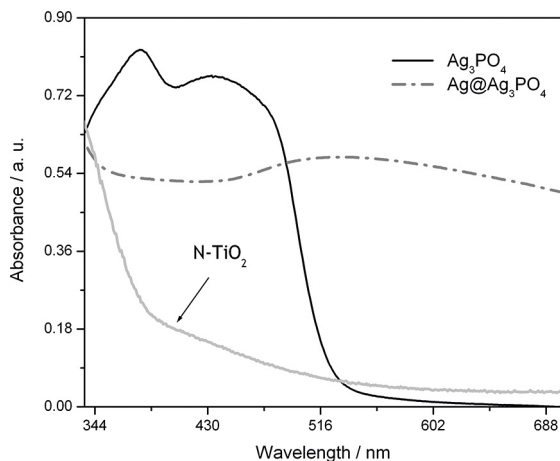


Figure 2. UV-vis diffuse reflectance spectra of the as-prepared Ag₃PO₄, Ag₃PO₄/Ag and N-TiO₂ samples.

with that of O 2p, and it leads to the dominant transitions at the absorption edge those from N 2p_π to Ti d_{xy}, instead of from O 2p_π as occurred in TiO₂. As can be seen, pure Ag₃PO₄ exhibits a steep absorption edge in the UV and visible range shorter than 530 nm. According to the previous document¹⁶, the strong absorption below a wavelength of 530 nm is associated with the optical band gap of Ag₃PO₄. The indirect band gap of Ag₃PO₄ is estimated to be 2.32 eV, as well as, direct transition is 2.40 eV. Moreover, the absorption curve shows no additional absorption traces or splitting of bands due to localized levels in the bandgap, indicative of the high quality of Ag₃PO₄ and from the viewpoint of oxygen vacancies and metal impurities. In the case of the Ag₃PO₄/Ag composite, the absorbance at the range of 500-800 nm is higher than that of pure Ag₃PO₄, which is attributed to the characteristic absorption of surface plasmon resonance (SPR) of metallic silver on Ag₃PO₄ surface and Ag nanoparticles should be larger than at least 30 nm to efficiently absorb long wavelength of visible light. This resonance is a consequence of enhancement of local electromagnetic field due to the resonant response of the metal electrons at specific wavelengths, which strongly depends on the morphology and size of the metal nanoparticles, composition, as well as the dielectric properties of the surrounding medium. For this reason, the improved light absorption for visible light is ascribed to silver nanoparticles with localized surface plasmonic resonance, which indicates that silver nanoparticles were reduced from silver ions on the outer surface of silver orthophosphate.

PL emission spectra can be carried out to study the efficiency of charge carrier trapping, immigration and transfer, and to understand the fate of photo-generated electrons and holes in semiconductor. Since photoluminescence (PL) emission is mainly due to the combination of excited electrons and holes, PL is thus an effective approach for obtaining information about the surface vacancies, and the

migration and separation efficiency of the photo-generated charge carriers, as it is known that the rate of electron-hole recombination is one of the most important factors affecting the photocatalytic activity. The weaker PL intensity, the bigger possibility of photoexcited charge carrier separation. The room temperature PL emission spectra of the as-prepared pure Ag_3PO_4 nanoparticles and $\text{Ag}_3\text{PO}_4/\text{Ag}$ nanocomposite with the excitation wavelength of 280 nm are compared and illustrated in Figure 3. From the spectra of pure Ag_3PO_4 nanoparticles and the $\text{Ag}_3\text{PO}_4/\text{Ag}$ nanocomposite, it can be observed that two samples exhibited the similar emission peaks in the visible-light range. The strong emission around 420 nm is supposed to arise from the recombination of the charge-transfer transition between the $\text{O}2p$ orbital and the empty d orbital of the central Ag^+ or of the self-trap excitons in the PO_4 oxyanion complex¹⁷. The broad PL band centered at 500 nm is considered to originate from the radiative recombination of photo-generated holes with electrons around the surface oxygen vacancy. The emission at about 530 nm, which has a photon energy approximately equal to the band gap of Ag_3PO_4 , is caused by the photoexcited electrons at the conduction band edge recombining with holes at the valence band edge. Meanwhile, the overall emission intensity from the $\text{Ag}_3\text{PO}_4/\text{Ag}$ nanocomposite is obviously weakened compared with that of pure Ag_3PO_4 nanoparticles, indicating that the deposited metallic Ag can be used as electron scavengers to suppress the recombination of charge carriers and thus result in PL quenching. By comparison, the emission peak of pure Ag_3PO_4 higher than that of $\text{Ag}_3\text{PO}_4/\text{Ag}$ which implied that the addition of metallic silver reduced the electron-hole recombination rate. Therefore it can improve the efficiency of Ag_3PO_4 . The quenching effect can be explained in the terms of the interfacial charges transfer from Ag_3PO_4 to Ag nanoparticles. Therefore, the introduction of Ag nanoparticles onto surface of Ag_3PO_4 is favorable to separate photogenerated charge carriers. The efficient charge

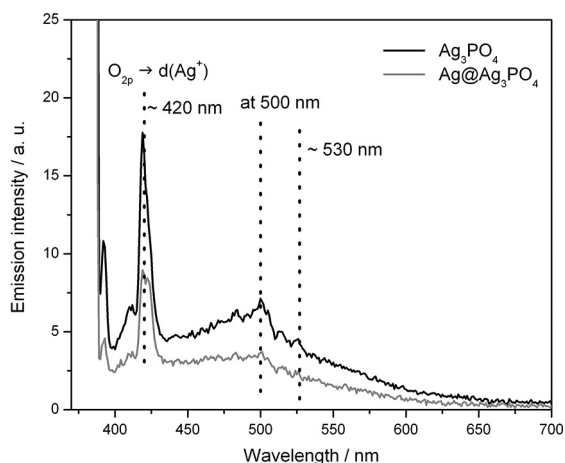


Figure 3. Room temperature photoluminescence spectra of the as-prepared pure Ag_3PO_4 nanoparticles and $\text{Ag}_3\text{PO}_4/\text{Ag}$ nanocomposite.

separation can lengthen the lifetime of the charge carriers and may notably improve the photocatalytic performance.

The transient photocurrent responses of the $\text{Ag}_3\text{PO}_4/\text{ITO}$ and $\text{Ag}_3\text{PO}_4/\text{Ag}/\text{ITO}$ electrodes can be recorded via several on-off cycles of irradiation to give further evidence for the visible light activity of the as-prepared photocatalysts. Figure 4 depicts the current-voltage curves for $\text{Ag}_3\text{PO}_4/\text{ITO}$ and $\text{Ag}_3\text{PO}_4/\text{Ag}/\text{ITO}$ under three on/off visible-light irradiation cycles. It can be seen that the photocurrent rapidly decreases to zero as long as the light was turned off, and the photocurrent remained a constant value when the light was on. The reducibility of these results is very good. For each sample, an anodic photocurrent peak, which decayed rapidly followed by a steady current, appears at the initial time of irradiation. When the light is switched off, a cathodic peak can also be observed. The initial current is due to the separation of electron-hole pairs at the semiconductor/electrolyte interface: holes are trapped or captured by reduced species in the electrolyte, while the electrons are transported to the back contact substrate. The decay of the photocurrent indicates that a fraction of the holes reaching the semiconductor surface, instead of capturing electrons from the electrolyte, either recombines with electrons from the conduction band and/or accumulates at the surface. After recombination of the excessive holes with electrons, the generation and transfer of electron-hole pairs reach an equilibration and form a constant current. When the light is interrupted, the holes accumulated in the surface state still continue to recombine, and a cathodic peak is observed. It is clear that each sample was prompt in generating photocurrent with a reproducible response to on/off cycles, demonstrating the effective charge transfer and successful electron collection for the samples within the photoelectrochemical cell (PEC) responses. The rise and fall of the photocurrent corresponds well to the illumination being switched on and off. In comparison with pure Ag_3PO_4 , $\text{Ag}_3\text{PO}_4/\text{Ag}$ exhibited an increased photocurrent density. The photocurrent density of the $\text{Ag}_3\text{PO}_4/\text{Ag}/\text{ITO}$ is greater than 0.35 mA cm^{-2} , whereas that of $\text{Ag}_3\text{PO}_4/\text{ITO}$ is only 0.12 mA cm^{-2} . The photocurrent of the $\text{Ag}_3\text{PO}_4/\text{Ag}$ is about three times as high as that of pure Ag_3PO_4 sample, indicate enhanced photoinduced electron and hole separation. As a result, the recombination rate of the photogenerated electron-hole pairs is greatly reduced by the deposited Ag nanoparticles. The separation and transfer of electron and hole pairs can be also analysed using electrochemical impedance spectroscopy (EIS). The radius of the arc on the EIS Nyquist plot reflects the reaction rate occurring at the surface of electrode. The smaller the radius of the EIS Nyquist plot, the lower the electric charge-transfer resistance is. As shown in Figure 5, the arc radius of the $\text{Ag}_3\text{PO}_4/\text{Ag}/\text{ITO}$ is smaller than that of the $\text{Ag}_3\text{PO}_4/\text{ITO}$ under visible light irradiation, which suggests that having metallic Ag nanoparticles on the $\text{Ag}_3\text{PO}_4/\text{ITO}$ leads to a more effective separation of photo-generated electron-hole pairs and faster interfacial charge

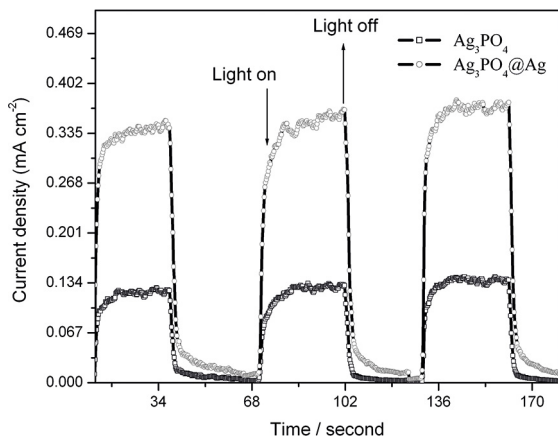


Figure 4. Transient photocurrent response of the as-prepared Ag₃PO₄/ITO and Ag₃PO₄/Ag/ITO under visible light irradiation.

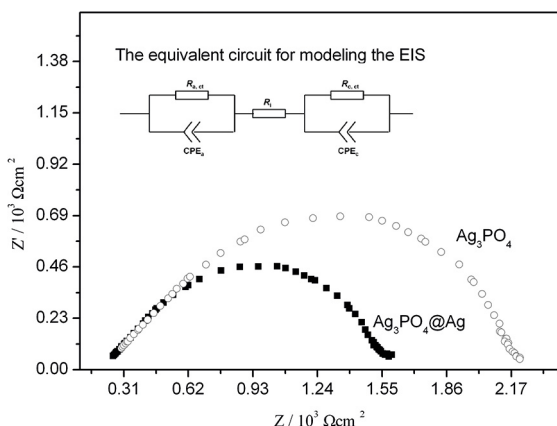


Figure 5. EIS Nyquist plots of the as-prepared Ag₃PO₄/ITO and Ag₃PO₄/Ag/ITO under visible light irradiation.

transfer. The decrease in the charge-transfer resistance of Ag₃PO₄/Ag/ITO should be mainly ascribed to the fact that photogenerated electrons from Ag₃PO₄ can easily transfer to metallic silver, which induced the spatial separation of electron-hole pairs and prevent direct recombination. These results prove that metallic Ag nanoparticles deposited onto the Ag₃PO₄/ITO can promote the transfer of photo-generated electrons, inhibiting the recombination of electrons and holes effectively, which would contribute more significantly to the remarkable enhancement of photocatalytic activity.

To evaluate and compare the visible-light photocatalytic activity of the as-prepared photocatalysts, the degradation of RhB dye under visible light irradiation was performed. The maximum wavelength absorption of RhB in neutral form under visible light is at about 553 nm, therefore the variation of methyl orange absorbance at maximal wavelength was detected. Figure 6(a)–(c) demonstrate the photodegradation course of RhB by the reference N-TiO₂, Ag₃PO₄ and Ag₃PO₄/Ag samples, respectively. As is displayed, the as-prepared Ag₃PO₄/Ag sample shows the highest photocatalytic efficiency compared to that of the reference N-TiO₂ and Ag₃PO₄. An

approximate 100% degradation of RhB was achieved within 40 min under visible light illumination, while the degradation percentage of RhB were 42% and 58% for the reference N-TiO₂ and Ag₃PO₄ samples at the same period, respectively. The enhancement of the degradation phenomenon of Ag₃PO₄/Ag sample could be attributed to the deposited Ag nanoparticles, which have an influence on the surface charge distribution of Ag₃PO₄, which can promote the transfer of photo-generated electrons, restraining the recombination of electrons and holes effectively. Because Ag₃PO₄/Ag sample showed the highest photocatalytic activity, controlled degradation experiments for Ag₃PO₄/Ag sample were carried out. In this regard, the photocatalytic reactivity of the Ag₃PO₄/Ag hybrid was studied by monitoring the degradation process of a mixed-organics aqueous solution containing phenol and X-3B dye in the presence of Ag₃PO₄/Ag under visible-light illumination. To simulate real polluted water in some degree, we thus mixed the above dyes involving phenol (10.0 mg/L) and X-3B (20.0 mg/L). Phenol and X-3B were chosen as model pollutants because their spectral overlap is relatively slight and their some characteristic absorption peaks are also separated. Figure 6(d) shows the temporal evolution of the spectral changes upon the photo-decomposition of mixed-organics aqueous solution over the Ag₃PO₄/Ag hybrid. It could be seen that the characteristic absorption of X-3B dye or phenol around 525 or 270 nm decreased with the increase of irradiation time. The effective photocatalytic degradation of this mixture by Ag₃PO₄/Ag shows the universality of Ag₃PO₄/Ag as a photocatalyst, indicating the potential merit in practical use. This capability makes the Ag₃PO₄/Ag hybrid a promising candidate for wide applications in the environmental purification.

3.1. Photocatalytic mechanism

It is generally accepted that organic pollutants can be photodegraded via photocatalytic oxidation (PCO) process and different quenchers should be added into the reaction mixture to verify the active center and deduce the mechanism. A large number of main reactive oxygen species (ROSs) including h⁺, •OH and •O₂⁻ involved in PCO process. Therefore, radical and hole trapping experiments were performed to detect the main oxidative species in the PCO process to reveal the photocatalytic mechanism. The photogenerated electron–hole pairs in the photocatalytic process could be detected through trapping experiments of radicals and holes by using scavengers. Benzoquinone (BQ), sodium azide (NaN₃), dimethylsulfoxide (DMSO) and ethylenediaminetetraacetic acid sodium (EDTA-2Na) could be used as scavenging species in order to investigate the generation and roles of •O₂⁻, ¹O₂, •OH and h⁺, respectively¹⁸. In the present study, 0.2 mM of BQ, NaN₃, DMSO and EDTA-2Na were added as scavengers on the degradation of phenol in attempt to elucidate the reaction mechanism over

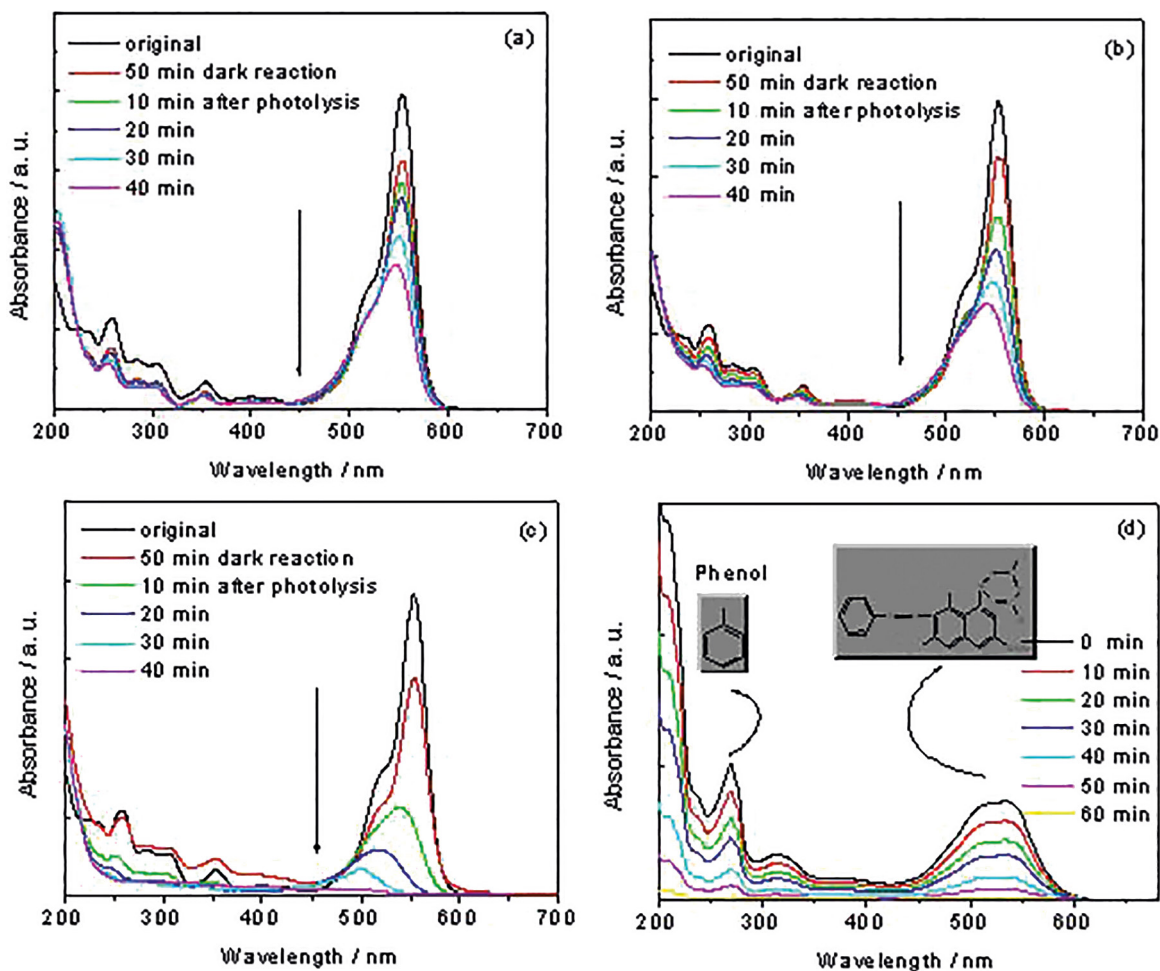


Figure 6. Temporal evolution of the UV-vis spectral changes upon the photodegradation of RhB over (a) N-TiO₂, (b) Ag₃PO₄, (c) Ag₃PO₄/Ag, and (d) photodegradation of an aqueous solution containing a mixture of phenol and X-3B dye over Ag₃PO₄/Ag hybrid as a function of irradiation time.

the visible-light responsive Ag₃PO₄/Ag. As is shown in Figure 7a, compared with no scavenger at the same condition, the photocatalytic activity in the Ag₃PO₄/Ag system is greatly suppressed by the addition of DMSO (\bullet OH radical scavenger) and EDTA-2Na (hole scavenger), indicate the main roles of \bullet OH and h⁺ for MO degradation. The addition of BQ (\bullet O₂⁻ radical scavenger) and NaN₃ (¹O₂ scavenger) showed weaker effects in PCO process of phenol, suggesting that \bullet O₂⁻ and ¹O₂ played comparatively minor role for phenol degradation. The result shows that the degradation of phenol was inhibited in the presence of these scavengers with the order of significance following DMSO > EDTA-2Na > NaN₃ > BQ. Thus, it is postulated that \bullet OH followed by h⁺ significantly contributed to the degradation of phenol, while the roles of \bullet O₂⁻ and ¹O₂ was less significant. In order to further confirm the existence of \bullet OH, the \bullet OH which formed on a photo-illuminated Ag₃PO₄/Ag catalysts surface was detected by a photoluminescence (PL) method using terephthalic acid (TA) as a probe molecule. The experimental conditions were the

same as the photocatalytic reaction system and the results are shown in Figure 8. It can be seen that Ag₃PO₄/Ag can produce \bullet OH after illuminated for certain time of visible time and the fluorescence intensity of PL signal at 425 nm increases along with irradiation time. This suggests that the fluorescence is caused by chemical reactions of TA with \bullet OH formed in photocatalytic reaction, while the fluorescence intensity was proportional to the amount of \bullet OH produced. Hence, \bullet OH is the reactive oxygen species in Ag₃PO₄/Ag system and finally induces the degradation of phenol. Generally, two competitive processes, charge carriers recombination versus interfacial charge transfer, may occur after the creation of photo-generated charge carriers. The former eliminated the photo-generated electrons and holes, while the latter produced active radical species (e.g. \bullet OH, \bullet O₂⁻, H₂O₂). The results suggest that in situ loading Ag nanoparticles on the surface of Ag₃PO₄ is a good way to accelerate the transfer and separation of the photoinduced carriers, which leads to a high photocatalytic activity. For the Ag₃PO₄-based catalysts,

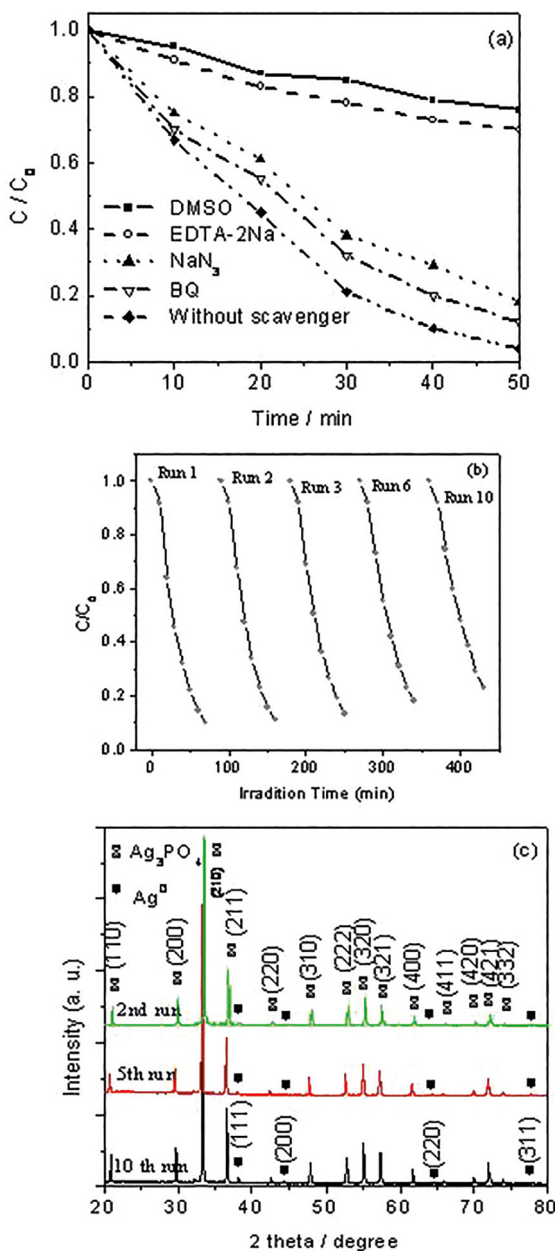


Figure 7. Photocatalytic degradation of phenol (a) using Ag₃PO₄/Ag under visible-light irradiation without and with the presence of various scavengers, (b) cycle experiments upon phenol degradation to test the reusability of the Ag₃PO₄/Ag hybrid and (c) XRD patterns of Ag₃PO₄/Ag hybrid gained after photocatalytic reactions for successive experimental runs.

the valence band edge potential of Ag₃PO₄ is 2.81 eV, the potential of OH[•]/•OH couple is 2.7 eV¹⁹. Under visible light irradiation ($\lambda > 420$ nm) photo-generated electron-hole pairs emerge from the photoexcited Ag₃PO₄ semiconductor. Thus, some of the photo-generated holes accumulated in Ag₃PO₄ could interact with surface-bound H₂O or OH⁻ to produce the •OH species. Because of the lower conduction band edge potential of Ag₃PO₄ (0.45 eV), the photo-induced

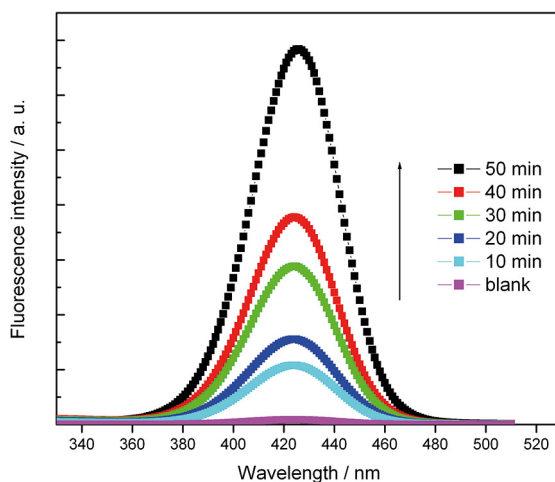


Figure 8. PL spectral changes with visible-light irradiation time for the Ag₃PO₄/Ag hybrid in 3.0×10^{-4} M basic solution of terephthalic acid.

electrons could not provide a sufficient potential to reduce O₂ to •O₂⁻ (the redox potential of O₂/•O₂⁻ is 0.13 eV) through the one-electron reduction process and further generate •OH. Therefore, it is reasonable for O₂ to combine with electrons trapped by noble Ag nanoparticles and form H₂O₂ (O₂ + 2H⁺ + 2e⁻ → H₂O₂) via a two-electron reduction reaction process (E(O₂/H₂O₂) = +0.695 V/NHE). Then the formed H₂O₂ quickly reacts with an electron to finally generate •OH (H₂O₂ + e⁻ → •OH + OH⁻). Therefore, highly oxidative species, such as •OH and holes are produced, which then reacted with MO in solution. A possible mechanism can be proposed to explain the high photocatalytic activity of the as-prepared Ag₃PO₄/Ag plasmonic nanocatalyst. The visible light can be absorbed efficiently by both the Ag₃PO₄ and the plasmon-excited silver nanoparticles (Ag^{*})²⁰. Electrons in the valence band of Ag₃PO₄ could be excited to the conduction band and a large amount of electron-hole pairs are then generated. The electrons generated from Ag₃PO₄ can transfer quickly towards Ag nanoparticles, so that the Ag⁺ of the Ag₃PO₄ nanocatalyst can escape from the reduction by these excess electrons to the maximum extent, which ensures the stability of the catalyst. The holes generated on Ag₃PO₄ could then oxidize the dyes molecule directly or interact with surface-bound H₂O or OH⁻ to produce the •OH species. The degradation of dyes was mainly governed by the highly oxidative species •OH or holes, which has been proved experimentally above. Part of the excess electrons in the conduction band of Ag₃PO₄ could transfer to the Ag nanoparticles when they behave as the electron acceptor. In this regard, metallic Ag formed by reduction of Ag⁺ in Ag₃PO₄ works as plasmonic photocatalyst as well as electron storage to make Ag₃PO₄ materials with improved photocatalytic performance or stability by modification. It should be pointed out that dye is a complex molecule, its degradation and oxidation are not straightforward usually. Therefore it is

not very suitable as a model substrate since dye can sensitize photocatalyst under visible light more or less. Nonetheless, preliminary results indicate that target dye can almost not be removed itself only by visible illumination in the absence of catalyst, which confirming that the visible activity is due to the photocatalyst rather than the dye sensitization effect.

To evaluate the structural stability, the crystalline structures of $\text{Ag}_3\text{PO}_4/\text{Ag}$ nanohybrid after several cycle experiments for phenol degradation were studied (as shown in Figure 7c). It can be seen that a small diffraction peak of metallic silver (Ag) appeared in the XRD pattern of the as-prepared $\text{Ag}_3\text{PO}_4/\text{Ag}$ after the second cycle experiment, indicating that the reduction of a small quantity of Ag_3PO_4 into metallic Ag particles has taken place during the phenol degradation process. Overall, the (111) diffraction peak of silver increases slightly with repeat times. However, no evident crystalline structure changes could be observed in the XRD pattern of $\text{Ag}_3\text{PO}_4/\text{Ag}$ nanohybrid during multiple cycle experiments, indicating that silver nanoparticles improved the stability of the Ag_3PO_4 photocatalyst. Actually, the repeatability test should be done with increasing times to delicately figure out the silver reduction or oxidation behavior along with the silver's disappearing (111) peak, whereas the protection effect providing by silver might also decay for the latter situation. It was demonstrated in Figure 7c that the presence of a small quantity of metallic Ag comes from the partial reduction of silver compound under visible light irradiation. These Ag^0 species might be used as protective coatings that inhibit the further photocorrosion of Ag_3PO_4 and maintain the structural stability as well as the photocatalytic efficiency, photocatalytic performance displays no significant loss after the reaction is performed consecutively ten times, as shown in Figure 7(b). This result clearly hints that the structural stability of Ag_3PO_4 is improved with the introduction of Ag^0 species, because the deposited Ag^0 species played a role to impede the self-decomposition of Ag_3PO_4 . The phase content of a sample can be calculated from the integrated intensities of diffraction peaks from the XRD pattern. The weight fraction of metallic Ag (W_A) can be calculated from the equation below: $W_A = I_A / [I_A + (I_B/K_0)]$, here I_A and I_B represent the integrated intensity of the Ag peaks and Ag_3PO_4 peaks, respectively. K_0 represents the specific value of reference intensity ratio (RIR) of Ag_3PO_4 and Ag, which is determined to be 2.66²¹. The calculated weight fraction of metallic Ag (W_A) for $\text{Ag}_3\text{PO}_4/\text{Ag}$ hybrid after first experimental runs is 7.2%, which is slightly lower than that of the calculated weight fraction of metallic Ag (W_A) for $\text{Ag}_3\text{PO}_4/\text{Ag}$ hybrid after 10th successive experimental runs (8.6%), which may explain why the photocatalytic activity displays no evident drop even it be reused ten times.

Considering the surface plasmon resonance (SPR) of the Ag nanoparticles, the photo-induced h^+ on silver nanoparticles can also oxidize the dye molecule directly. In addition, the excellent conductivity of the silver nanoparticles enhances

the interfacial charge transfer and stops the recombination of electron-hole pairs effectively. Then the excess electrons accumulating on the surface of Ag nanoparticles will go to reduce the dye molecules, or are trapped by O_2 and H_2O at the surface of photocatalyst in the solution to form O_2^- or $\bullet\text{O}_2^-$ reactive oxygen species. These reactive oxygen species also help degrade the dye molecules in some degree. Meanwhile, the dye molecules are excited by the absorption of visible light, and electrons are injected into the conduction band of Ag_3PO_4 or the silver nanoparticles, facilitating the oxidation of the dye molecules. Part of the excess electrons in the conduction band of Ag_3PO_4 will further transfer to the Ag nanoparticles, which behave as the electron acceptor. As is known, metallic Ag^0 can serve as an excellent electron acceptor and efficient trap the photoinduced electrons. Therefore, the localized surface plasmon resonance produced by the collective oscillations of surface electrons on the Ag^0 species could induce an enhancement of the local inner electromagnetic field. Due to the local electromagnetic field and the excellent conductivity of the Ag^0 species, the photoinduced electrons can be transferred quickly to the Ag^0 species, instead of remaining in the Ag^+ ions of the Ag_3PO_4 lattice. These electrons trapped by Ag^0 species will further react with the O_2 molecules adsorbed on the surface of the composite to form active $\bullet\text{OH}$ radicals. Therefore, the further reduction of Ag_3PO_4 could be inhibited. Moreover, photogenerated holes tend to remain on the surface of Ag_3PO_4 due to that PO_4^{3-} ions have large negative charge which prefers to attract holes and repel electrons. Meanwhile, PO_4^{3-} ions on the surface of Ag_3PO_4 have strong bonding ability with H_2O . As a result, H_2O could be adsorbed on surface easily and then oxidized by the holes to $\bullet\text{OH}$, which eventually oxidize dye to carbon dioxide or small molecules. During the degradation of dye pollutants, some organic radicals or active oxidizing species could be also formed following the photo-induced electron injection from the dyes into Ag_3PO_4 , which could attack other co-existing pollutants to provoke their decontamination under visible light irradiation. Finally, we stress that the transfer of the electrons from both the dyes and the conduction band of Ag_3PO_4 into the silver nanoparticles avoids the capture by Ag^+ of Ag_3PO_4 , which ensures the stability of the composite catalyst, so the $\text{Ag}_3\text{PO}_4/\text{Ag}$ hybrid could show efficient activity and remain stable without deterioration. Those results strongly support that the structural stability of Ag-based materials can be markedly enhanced by metallic Ag.

4. Conclusions

In summary, a highly efficient and stable $\text{Ag}_3\text{PO}_4/\text{Ag}$ hybrid photocatalyst was prepared using an in situ photoinduced method with the assistance of Na_3Cit at room temperature. The as-prepared $\text{Ag}_3\text{PO}_4/\text{Ag}$ exhibited excellent performance on the degradation of RhB dye or phenol/X-3B mixture and

displayed much higher photocatalytic activity than single Ag₃PO₄ or N-doped TiO₂ under visible light ($\lambda > 420$ nm). After ten cycles of repetition tests, the degradation efficiency and structural stability was remain efficient and stable. Photocatalytic mechanism investigations demonstrate that the degradation of phenol over the as-prepared Ag₃PO₄/Ag under visible light is mainly via $\bullet\text{OH}$ and h^+ oxidation mechanism. The Ag₃PO₄/Ag hybrid is a promising candidate for the removal of hazardous organic materials from wastewater. In addition, this work not only promotes the development of Ag₃PO₄ for practical applications, but also inspires the exploration of similar facile methods to stabilize other easily photocorroded catalysts.

5. Acknowledgments

This work was supported by the Natural Science Foundation of Hubei Province of China (2011CDB148).

6. References

1. Zhang JL, Wu YM, Xing MY, Leghari SAK, Sajjad S. Development of modified N doped TiO₂ photocatalyst with metals, nonmetals and metal oxides. *Energy & Environmental Science*. 2010;3(6):715-726. DOI: 10.1039/B927575D.
2. Ajmal A, Majeed I, Malik RN, Idriss H, Nadeem MA. Principles and mechanisms of photocatalytic dye degradation on TiO₂ based photocatalysts: a comparative overview. *RSC Advances*. 2014;4(70):37003-37026. DOI: 10.1039/C4RA06658H.
3. Park H, Kim H, Moon GH, Choi W. Photoinduced charge transfer processes in solar photocatalysis based on modified TiO₂. *Energy & Environmental Science*. 2016;9(2):411-433. DOI: 10.1039/C5EE02575C.
4. Devi LG, Kavitha R. Review on modified N-TiO₂ for green energy applications under UV/visible light: selected results and reaction mechanisms. *RSC Advances*. 2014;4(54):28265-28299. DOI: 10.1039/C4RA03291H.
5. Kumar SG, Rao KSRK. Comparison of modification strategies towards enhanced charge carrier separation and photocatalytic degradation activity of metal oxide semiconductors (TiO₂, WO₃ and ZnO). *Applied Surface Science*. 2017;391(Pt B):124-148. DOI: 10.1016/j.apsusc.2016.07.081.
6. Kumar SG, Rao KSRK. Polymorphic phase transition among the titania crystal structures using a solution-based approach: from precursor chemistry to nucleation process. *Nanoscale*. 2014;6(20):11574-11632. DOI: 10.1039/C4NR01657B.
7. Devi LG, Reddy KM. Photocatalytic performance of silver TiO₂: Role of electronic energy levels. *Applied Surface Science*. 2011;257(15):6821-6828. DOI: 10.1016/j.apsusc.2011.03.006.
8. Qamar M. Photodegradation of acridine orange catalyzed by nanostructured titanium dioxide modified with platinum and silver metals. *Desalination*. 2010;254(1-3):108-113. DOI: 10.1016/j.desal.2009.12.006.
9. Devi LG, Reddy KM. Enhanced photocatalytic activity of silver metallized TiO₂ particles in the degradation of an azo dye methyl orange: Characterization and activity at different pH values. *Applied Surface Science*. 2010;256(10):3116-3121. DOI: 10.1016/j.apsusc.2009.11.083.
10. Zhang M, Li L, Zhang XT. One-dimensional Ag₃PO₄/TiO₂ heterostructure with enhanced photocatalytic activity for the degradation of 4-nitrophenol. *RSC Advances*. 2015;5(38):29693-29697. DOI: 10.1039/C4RA15946B.
11. Khan A, Qamar M, Muneer M. Synthesis of highly active visible-light-driven colloidal silver orthophosphate. *Chemical Physics Letters*. 2012;519-520:54-58. DOI: 10.1016/j.cplett.2011.11.015.
12. Indra A, Menezes PW, Schwarze M, Driess M. Visible light driven non-sacrificial water oxidation and dye degradation with silver phosphates: multi-faceted morphology matters. *New Journal of Chemistry*. 2014;38(5):1942-1945. DOI: 10.1039/C3NJ01012K.
13. Xu YS, Zhang WD. Morphology-controlled synthesis of Ag₃PO₄ microcrystals for high performance photocatalysis. *CrystEngComm*. 2013;15(27):5407-5411. DOI: 10.1039/C3CE40172C.
14. Panigrahy B, Srivastava S. Minuscule weight percent of graphene oxide and reduced graphene oxide modified Ag₃PO₄: new insight into improved photocatalytic activity. *New Journal of Chemistry*. 2016;40(4):3370-3384. DOI: 10.1039/C5NJ03118D.
15. Reunchan P, Umezawa N. Sulfur and Silicon Doping in Ag₃PO₄. *The Journal of Physical Chemistry C*. 2015;119(5):2284-2289. DOI: 10.1021/jp509715b.
16. Botelho G, Sczancoski JC, Andres J, Gracia L, Longo E. Experimental and Theoretical Study on the Structure, Optical Properties, and Growth of Metallic Silver Nanostructures in Ag₃PO₄. *The Journal of Physical Chemistry C*. 2015;119(11):6293-6306. DOI: 10.1021/jp512111v.
17. Zhang W, Hu C, Zhai W, Wang ZL, Sun YX, Chi FL, et al. Novel Ag₃PO₄/CeO₂ p-n Hierarchical Heterojunction with Enhanced Photocatalytic Performance. *Materials Research*. 2016;19(3):673-679. DOI: 10.1590/1980-5373-MR-2016-0009.
18. Sood S, Mehta SK, Umar A, Kansal SK. The visible light-driven photocatalytic degradation of Alizarin red S using Bi-doped TiO₂ nanoparticles. *New Journal of Chemistry*. 2014;38(7):3127-3136. DOI: 10.1039/C4NJ00179F.
19. Ghazalian E, Ghasemi N, Amani-Ghadim AR. Effect of gadollunium doping on visible light photocatalytic performance of Ag₃PO₄: Evaluation of activity in degradation of an anthraquinone dye and mechanism study. *Journal of Molecular Catalysis A: Chemical*. 2017;426(Pt A):257-270. DOI: 10.1016/j.molcata.2016.11.026.
20. Katsumata H, Taniguchi M, Kaneco S, Suzuki T. Photocatalytic degradation of bisphenol A by Ag₃PO₄ under visible light. *Catalysis Communications*. 2013;34:30-34. DOI: 10.1016/j.catcom.2013.01.012.
21. Dhanabal R, Chithambararaj A, Velmathi S, Bose AC. Visible light driven degradation of methylene blue dye using Ag₃PO₄. *Journal of Environmental Chemical Engineering*. 2015;3(3):1872-1881. DOI: 10.1016/j.jece.2015.06.001.